Spectrochimica Acta Part A: Molecular and Biomolecular Spectroscopy 117 (2014) 144–151

Contents lists available at ScienceDirect

Spectrochimica Acta Part A: Molecular and Biomolecular Spectroscopy

journal homepage: www.elsevier.com/locate/saa

Experimental and DFT studies on the vibrational and electronic spectra of 2-(1H-Imidazo [4,5-*f*][1,10]phenanthrolin-2-yl)phenol

Tingting Tang [a,b], Guodong Tang [a,b,*], ShanShan Kou [a,b], Jianyin Zhao [b], Lance F. Culnane [c,*], Yu Zhang [a,b]

[a] School of Chemical Engineering, Ningxia University, Ningxia 210094, PR China
[b] Jiangsu Key Laboratory for Chemistry of Low-Dimensional Materials, School of Chemistry and Chemical Engineering, Huaiyin Normal University, Huai'an 223300, Jiangsu Province, PR China
[c] UCB 215 Department of Chemistry and Biochemistry, University of Colorado at Boulder, Boulder, CO 80309, United States

HIGHLIGHTS

- The compound IPP was synthesized, structure was determined by X-ray diffraction.
- The structure, vibration and electronic spectra of the title had been studied.
- The calculated results and the experimental values agreed well.

GRAPHICAL ABSTRACT

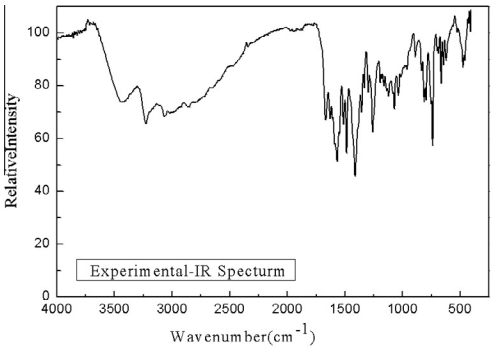

ARTICLE INFO

Article history:
Received 29 May 2013
Received in revised form 20 July 2013
Accepted 31 July 2013
Available online 9 August 2013

Keywords:
2-(1*H*-Imidazo [4,5-*f*][1,10] phenanthrolin-2-yl) phenol
X-ray diffraction technique
Vibration spectra
Electronic spectra

ABSTRACT

The compound 2-(1*H*-Imidazo [4,5-*f*][1,10] phenanthrolin-2-yl) phenol (IPP) was synthesized, followed by structure determination by X-ray diffraction, the results of which agree well with the calculated optimized, lowest energy geometrical structure. Vibrational information was obtained by FT-IR and Raman spectroscopy which also agree well with calculations (of harmonic vibration frequencies). The calculations were carried out with density functional theory B3LYP methods using 6-311G** and LANL2DZ basis sets. Absorption UV–Vis experiments of IPP in CH_3OH solution reveal three maximum peaks at 237.0, 274.0 and 335.0 nm, which are in agreement with calculated electronic transitions using TD-B3LYP/6-311G** in CH_3OH solution, and agree to a lesser extent with gas-phase calculations.

Introduction

The 1,10-phenanthroline ligands have played a particularly important role in the advancement of various supramolecular networks because of its imbedded π-electron system [1]. A series of 1,10-phenanthroline derivatives have been synthesized and characterized by UV–Vis, IR, ^{1}HNMR and elemental analysis [2–4]. Investigations of their applications have been reported in several disciplines of science, such as chemistry, physics, and material, as well as biological science [5,6]. The 1,10-phenanthroline ligand and its derivatives have attracted significant interdisciplinary attention because of their unique properties as chelating agents and common usage as ligands in metal–organic coordination polymers [7–11]. 1,10-Phenanthroline and substituted derivatives

* Corresponding authors. Address: Jiangsu Key Laboratory for Chemistry of Low-Dimensional Materials, School of Chemistry and Chemical Engineering, Huaiyin Normal University, Huai'an 223300, Jiangsu Province, PR China (G. Tang). Tel.: +86 517 83525318; fax: +86 517 83525320.
E-mail addresses: hysytanggd@hotmail.com (G. Tang), lanceculnane@gmail.com (L.F. Culnane).

1386-1425/$ - see front matter © 2013 Elsevier B.V. All rights reserved.
http://dx.doi.org/10.1016/j.saa.2013.07.108

play a key role in the performance of biological systems, such as antimalarial, antifungal, antitumoral, anti-allergic, anti-inflammatory and antiviral drugs [12–15]. It has also been used [16–20] in DNA-binding, DNA-photocleavage, third-order non-linear optical (NLO) materials, and asymmetric catalysis. The compound 2-(1*H*-Imidazo [4,5-*f*][1,10] phenanthrolin-2-yl) phenol (IPP) is one of the derivatives of 1,10-phenanthroline. The title compound has multiple binding sites (N, O) and has interesting optical properties. In order to present an in-depth study of IPP, we report a synthesis route, and in addition, the purpose for this work is (i) to determine the structure with X-ray diffraction and compare it to DFT calculations, (ii) to thoroughly study the vibration spectra of this molecule and to identify the various normal modes with the aid of HF and DFT studies, (iii) to compare the different DFT methods for the calculated vibration spectra, and (iv) to calculate the absorption bands in CH_3OH solution with an optimized geometry by using the time-dependent density functional theory (TDDFT) at B3LYP/6-311G**, B3LYP/LANL2DZ, HF/6-311G** and HF/LANL2DZ level associated with the polarized continuum model (PCM).

Experimental and computational section

Experimental

1,10-Phenanthroline-5, 6-dione 0.5302 g (2.5 mmol), 2-hydroxybenzaldehyde 0.4580 g (3.75 mmol) and ammonium acetate 3.8542 g (0.05 mol) were dissolved in glacial acetic acid. The mixture was refluxed for 2 h, and cooled to room temperature; it was then diluted with water and neutralized with concentrated aqueous ammonia; immediately a yellow precipitate was formed, which was washed with water. The compound was purified by recrystallization with glacial acetic acid and acetonitrile. The absorption UV–Vis spectrum in CH_3OH solution shows three maximum bands at 237.0, 274.0 and 335.0 nm.

A mixture of 0.0312 g (0.1 mmol) IPP, l mL (99%) triethylamine and 15 mL deionized water was sealed in a Teflon-lined stainless steel autoclave, and then heated at 160 °C for 72 h, and then cooled to room temperature. Colorless, transparent block-shaped crystals were obtained.

X-ray diffraction measurements of the crystal were performed on a Bruker Smart Apex CCD diffractometer at 296 K. The intensity data were collected using graphite monochromated Mo Kα radiation (λ = 0.71073 Å). The data collection 2θ range was 5.44–39.60°. No significant decay was observed during the data collection. The raw data were processed to give structure factors using the SAINT-plus program [21].

Empirical absorption corrections were applied to the data sets using the SADABS program [22]. The structure was solved by direction method and refined by full matrix least-squares against F^2 for all data using SHELXTL software [23]. All non-hydrogen atoms in the compound were anisotropically refined. All hydrogen atoms were included in the calculated positions and refined using a riding model with isotropic thermal parameters 1.2 times larger than those of the parent atoms. The crystal data, further details of the experimental conditions and the structure refinement parameters for the compound are given in Table 1 and the atomic numbering scheme is shown in Fig. 1.

The FT-IR spectrum of the title compound was recorded as KBr discs using an AVATAR 360 spectrophotometer in the range of 400–4000 cm^{-1} at room temperature. The Raman spectrum was recorded on a Bruker RFS 100/S FT-Raman spectrometer in the 50–3000 cm^{-1} regions with a diode-pumped air-cooled Nd-YAG laser source giving 1283 nm as an exciting line at 75 mW powers. The electronic spectra were recorded on a UV–Vis 916 spectrophotometer in the region of 200–800 nm using CH_3OH as the solvent.

Table 1
Crystal data and structure refinement for the title compound.

Empirical formula	$C_{19}H_{12}N_4O$
Formula weight	312.33
Temperature	296(2)
Radiation	Mo Kα (λ = 0.71073 Å)
Space group	*P*−1
a (Å)	9.920(3)
b (Å)	12.306(3)
c (Å)	12.444(4)
α (°)	89.173(4)
β (°)	78.586(4)
γ (°)	77.837(4)
V (Å^3)	1455.0(7)
Z	4
D_c/(g cm^{-3})	1.426
μ/mm^{-1}	0.093
Crystal size (mm)	0.2 × 0.2 × 0.15
θ range for data collection	1.67–25.00°
Index ranges	−11 ⩽ h ⩽ 11 −14 ⩽ k ⩽ 13 −14 ⩽ l ⩽ 14
Total reflections	10277
Goodness-of-fit on F2	1.007
R indices [$I > 2\sigma(I)$]	0.0563
R indices (all data)	0.1393
Largest difference peak and hole	0.18/−0.23

Methods of calculation

The geometry optimization proceeded in two steps; firstly, the initial geometry was constructed by MM+ molecular modeling with the HyperChem 6.0 package [24]. Secondly, the equilibrium geometry was optimized *ab initio* by restricted Hartree–Fock (HF) and density functional theory (DFT) B3LYP (Becke's three parameters hybrid method with the Lee, Yang and Parr non-local functions [25,26]) levels of theory with 6-311G** and LANL2DZ (Los Alamos ECP plus double-zeta) [27,28] basis sets. The structure was found to be a minimum since there is no imaginary frequency in the frequency calculation. Time-dependent density functional theory (TDDFT) [29] excited-state calculations were determined at the HF/6-311G**, HF/LANL2DZ, B3LYP/6-311G** and B3LYP/LANL2DZ level of theory both in gas phase and in CH_3OH solution. A polarizable continuum model (PCM) [30] including the solvent effect was chosen for excitation energy calculations. All calculations were performed using the Gaussian 09W program package [31]. All geometries converged perfectly. The vibrational frequencies and intensities were computed in a similar fashion.

Results and discussion

Molecular geometry

The optimized geometry with atomic numbering scheme for the title compound is shown in Fig. 1. Crystal data are summarized in Table 1. The selected experimental bond lengths and angles are given in Table 2. In the compound, the experimental bond length of C21–O27 (1.352(3) Å) is typical for a C–O single bond. The theoretical bond length of C–O was obtained by B3LYP/6-311G**, (1.342 Å), and HF/LANL2DZ, (1.361 Å), which agree well with the experimental value. The DFT (B3LYP/6-311G**, B3LYP/LANL2DZ) and HF (HF/6-311G**, HF/LANL2DZ) methods were used for geometrical optimization of the IPP molecule. The theoretical results show all atoms nearly co-planar, and all optimized bond lengths and angles agree well with the experimental values.

The optimized parameters of the title compound with DFT (B3LYP/6-311G**, B3LYP/LANL2DZ) and HF (HF/6-311G**, HF/LANL2DZ) methods are listed in Table 2. The overall magnitude

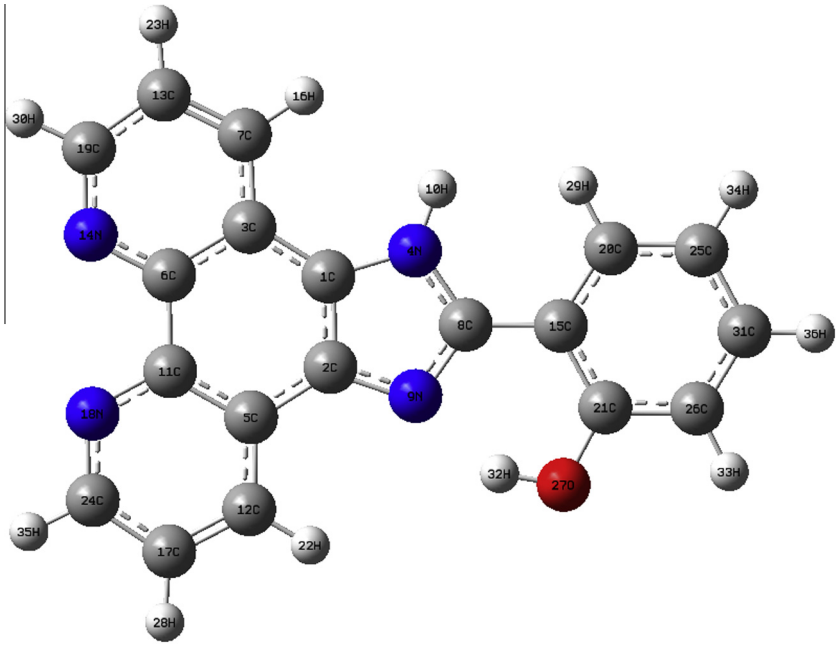

Fig. 1. Optimized geometry of the title compound.

Table 2
Optimized bond distances (Å) and bond angles (°) for the title compound with DFT and HF methods.

	Exp.	B3LYP/6-311G**	B3LYP/LANL2DZ	HF/6-311G**	HF/LANL2DZ
R(1,2)	1.370(4)	1.385	1.398	1.356	1.367
R(1,3)	1.421(4)	1.426	1.431	1.432	1.431
R(1,4)	1.377(3)	1.382	1.399	1.377	1.391
R(2,5)	1.430(4)	1.433	1.436	1.437	1.434
R(2,9)	1.384(3)	1.375	1.395	1.371	1.388
R(3,6)	1.409(4)	1.428	1.440	1.405	1.415
R(3,7)	1.401(4)	1.408	1.421	1.401	1.410
R(4,8)	1.356(3)	1.375	1.390	1.357	1.373
R(5,11)	1.413(4)	1.423	1.436	1.400	1.411
R(5,12)	1.400(4)	1.406	1.419	1.401	1.409
R(6,11)	1.463(4)	1.471	1.477	1.472	1.471
R(6,14)	1.357(3)	1.346	1.368	1.334	1.351
R(7,13)	1.368(4)	1.378	1.393	1.365	1.377
R(8,9)	1.330(3)	1.329	1.354	1.299	1.319
R(8,15)	1.471(4)	1.455	1.456	1.470	1.465
R(11,18)	1.353(3)	1.347	1.369	1.336	1.352
R(12,17)	1.367(4)	1.378	1.393	1.364	1.377
R(13,19)	1.387(4)	1.405	1.420	1.401	1.409
R(14,19)	1.327(3)	1.322	1.342	1.301	1.319
R(15,20)	1.381(4)	1.406	1.418	1.398	1.406
R(15,21)	1.391(4)	1.420	1.431	1.401	1.406
R(17,24)	1.397(4)	1.406	1.420	1.402	1.411
R(18,24)	1.318(4)	1.322	1.343	1.300	1.319
R(20,25)	1.375(4)	1.384	1.399	1.373	1.384
R(21,26)	1.390(4)	1.401	1.411	1.394	1.398
R(21,27)	1.352(3)	1.342	1.372	1.329	1.361
R(25,31)	1.367(4)	1.399	1.415	1.392	1.402
A(1,2,5)	120.8(3)	120.9	121.1	121.1	121.4
A(4,8,9)	112.1(3)	110.5	109.9	111.2	110.3
A(4,8,15)	124.7(3)	125.1	126.4	124.0	124.9
A(6,14,19)	117.7(3)	118.9	119.1	119.3	120.1
A(15,21,27)	122.8(3)	122.9	121.9	123.7	123.0
A(26,21,27)	117.5(3)	117.8	118.3	116.9	116.8
D(4,1,3,7)	2.0(2)	0.0	0.0	−0.0	0.0
D(3,1,4,8)	2.4(2)	180.0	180.0	180.0	180.0
D(2,5,11,18)	1.3(2)	180.0	180.0	−180.0	180.0
D(14,6,11,18)	0.8(2)	0.0	0.0	0.0	0.0
D(8,15,21,27)	1.9(3)	0.0	0.0	0.3	0.0
D(12,17,24,18)	1.9(3)	0.0	0.0	0.0	0.0

of the bond lengths listed in decreasing order for each calculation method are: B3LYP/LANL2DZ > B3LYP/6-311G** > HF/LANL2DZ > HF/6-311G**, which vary due to different exchange functions. The HF/LANL2DZ method pairing is found to predict bond length values most accurately. The B3LYP/LANL2DZ and HF/LANL2DZ methods give longer C21–O27 bond lengths than the experimental value, whereas B3LYP/6-311G** and HF/6-311G** methods give shorter C21–O27 bond lengths than the experimental value. The B3LYP/6-311G** and HF/LANL2DZ methods were found to predict bond length values more accurately overall and give values very close to the experimental value, for instance, 1.352(3) for C21–O27. In the imidazole ring, the experimental N9–C8, N9–C2, C1–C2, C1–N4, N4–C8 bond lengths are 1.330(3) Å, 1.384(3) Å, 1.370(4) Å, 1.377(3) Å, 1.356(3) Å, respectively, and the imidazole ring bond lengths agree well with the literature [32].

All the calculated N4-C8 bond lengths are slightly longer than the experimental value. Compared to the experimental value, the relative bond length errors are 1.34%, 2.46%, 0.06% and 1.26%, respectively, from B3LYP/6-311G**, B3LYP/LANL2DZ, HF/6-311G** and HF/LANL2DZ methods. Most of the calculated N9–C8 bond lengths are slightly lower than the experimental value. B3LYP/LANL2DZ gives a slightly larger-than-experimental-value. Compared to the experimental value, the relative bond length errors are −0.09%, 1.79%, −2.36% and −0.82%, respectively, from B3LYP/6-311G**, B3LYP/LANL2DZ, HF/6-311G** and HF/LANL2DZ methods. Most of the calculated N4–C1 bond lengths are slightly larger than the experimental value. HF/6-311G** gives a slightly lower-than-experimental-value. Compared to the experimental value, the relative bond length errors are 0.31%, 1.60%, −0.05% and 0.97%, respectively, from B3LYP/6-311G**, B3LYP/LANL2DZ, HF/6-311G** and HF/LANL2DZ methods. Both DFT and HF methods gave smaller values for the N4C8N9 angle than the experimental value, and the errors are 1.69% for the DFT method and 1.20% for HF method. Both DFT and HF methods gave larger values for the C2N9C8 angle than the experimental value, and the errors are 1.61% for the DFT method and 1.58% for HF method. All calculated values were within the experimental error. Table 2 shows that all the bond angles of the benzene ring and phenanthroline ring are close to 120°, which is very similar to the experimental value (118–125°). The theoretical results and experimental values all strongly suggest that the molecular structure of the compound is very co-planar.

Vibration assignments

The observed experimental FT-IR and FT-Raman spectra are shown in Fig. 2. Experimental and calculated vibrational frequencies (cm^{-1}) by DFT and RHF methods are listed in Table 3. Calculated IR spectra are shown in Fig. 3. Gaussview program [33] was used to assign the calculated harmonic frequencies. The vibrational frequencies obtained by the B3LYP/6-311G** method show the coupling phenomenon of each bond coordinates. The equation of the scaling by the b3lyp/6-311g** method is $y = 1.055–74.29355x$, and the correlation $R = 0.99579$; and the equation of the scaling by the b3lyp/lanl2dz method is $y = 1.04242–40.48219x$, and the correlation $R = 0.99612$.

C–H vibrational modes

The IR bands of benzene ring stretching vibrations are expected to appear in the 3000–3100 cm^{-1} frequency range. The strong IR band at 3067 cm^{-1} is assigned to a benzene ring stretching vibration of IPP. No band corresponding to this vibration is observed in the Raman spectrum. The B3LYP/6-311G** calculations expect the C–H stretching vibration of benzene ring to be at 3138.78–3199.05 cm^{-1}. Compared with the experimental values, the

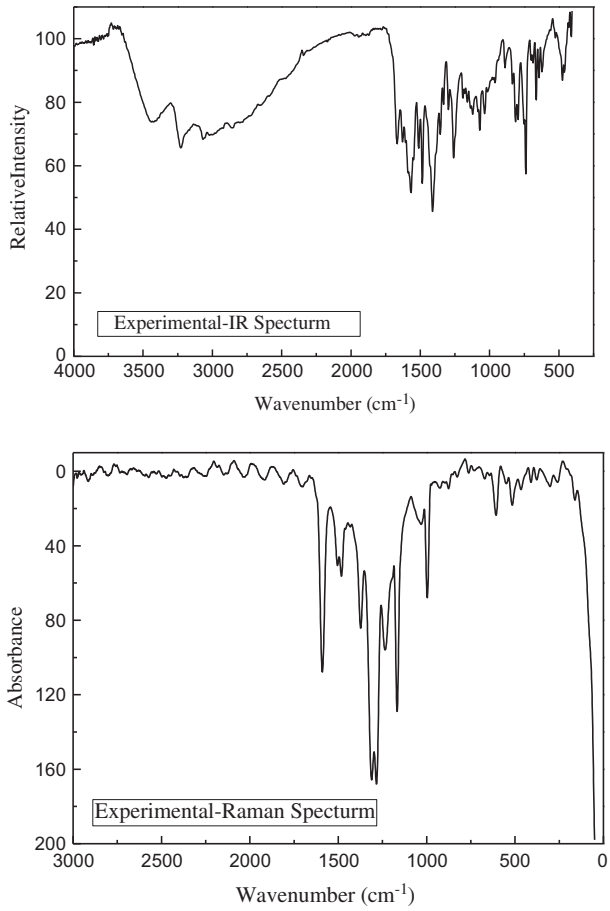

Fig. 2. Experimental FT-IR and FT-Raman spectra for the title compound.

B3LYP/6-311G** overestimate the frequency with an error less than 4.3%.

The observed bands at 1160 cm^{-1} and 1192 cm^{-1} in the IR spectrum and 1167 cm^{-1} in the Raman spectrum are assigned to in-plane C–H bending of the benzene ring, and the computed values are: 1139.40, 1184, and 1213.67 cm^{-1}, with errors of 1.8%, 0.7% and 1.8%. These theoretical values match the experimental values better than the aforementioned benzene ring stretching vibrations. The observed bands at 1036 and 1070 cm^{-1} in the IR spectrum and 996 cm^{-1} in the Raman spectrum are assigned to in-plane C–H bending of the R2 (ring of C3C6N14C19C13C7) and R3 (ring of C5C11N18C24C17C12) benzene ring, and the B3LYP/6-311G** calculation yields frequencies at 1086.94 and 1088.06 cm^{-1}, with errors of 4.7% and 1.7%.

The observed bands at 812 and 835 cm^{-1} is assigned to out-of-plane C–H wagging on the benzene ring (812 and 827 cm^{-1} have reported [7]). There is no band corresponding to this vibration in the Raman spectrum. The theoretical values are 807.60 and 826.09 cm^{-1} with an error of 0.6% and 1.1%. A strong IR band at 1411 cm^{-1} is assigned to in-plane C–H wagging of the benzene ring. The band is weakly coupled with the stretching vibration of the benzene ring. The theoretical values give 1439.63, 1444.67 and 1462.81 cm^{-1} with errors of 2.0%, 2.3% and 3.6%.

Ring modes

The IR bands at 1485, 1511, 1627, and 1666 cm^{-1} are mainly due to the C–C stretching vibration of phenyl ring and imidazole ring [34]. The band is strongly coupled with C–H wagging in-plane of the phenyl ring and O27H wagging, also in-plane. Two strong Raman bands corresponding to the bands are observed at 1482,

Table 3
Experimental and calculated vibrational frequencies (cm^{-1}) with DFT and RHF methods.

No.	B3LYP/6-311G**	B3LYP/LANL2DZ	Exp. (IR)	Exp. (Raman)	Assign.
1	21.28(0.19)	38.67(1.04)			ωR5
2	45.00(0.02)	48.12(0.00)			ωR5
3	82.47(0.25)	81.34(0.33)			ρR5
4	91.10(4.40)	95.80(7.91)			ωR2 + ωR3 + ωR5
5	96.90(1.04)	107.03(0.15)			ωR2 + ωR3 + ωR5
6	123.73(0.03)	131.25(0.10)			ωR2 + ωR3 + ωR5
7	178.92(5.20)	193.91(4.57)			τR2 + τR3 + τR4
8	199.94(0.95)	198.81(1.26)			ρR2 + ρR3
9	208.04(0.00)	219.11(9.17)			τR2 + τR3 + τR4 + τR5
10	220.919(7.80)	220.36(0.00)			ρR4 + ρR5
11	271.76(1.98)	270.40(3.30)			ρR2 + ρR3
12	277.91(0.76)	283.38(1.09)			τR1 + τR2 + τR3 + τR5
13	312.28(0.71)	323.54(0.75)			τR1 + τR2 + τR3 + τR4
14	357.02(1.09)	374.44(0.45)			τR1 + τR2 + τR3 + τR4 + τR5
15	411.54(4.69)	411.11(3.86)			νR1
16	418.36(1.19)	421.29(1.49)			ρR4 + ρC21O27
17	425.90(24.27)	451.93(0.37)			ωN4H + τR5
18	447.68(3.29)	452.89(0.00)			ωN4H + τR1 + τR2 + τR3
19	453.55(0.74)	475.35(2.45)			νR1 + ρC21O27
20	481.40(10.94)	478.88(3.50)			ωN4H + τR1 + τR2 + τR3 + τR5
21	481.52(1.66)	500.53(0.00)			νR1 + νR5
22	490.13(28.19)	527.43(10.45)	475(86.88)		ωN4H + τR1 + τR2 + τR3 + τR5
23	533.30(9.41)	551.71(1.07)			ρR5
24	544.07(4.16)	565.95(4.92)			τR1 + τR2 + τR3 + τR5
25	557.95(0.27)	580.55(4.50)			τR1 + τR2 + τR3 + τR4 + τR5
26	570.61(4.55)	603.51(1.89)			νR5
27	585.20(0.02)	621.65(3.33)			τR2 + τR3
28	625.92(3.63)	626.55(74.18)			νR1 + νR2 + νR3 + νR5 + ρR4
29	648.49(10.56)	649.64(11.85)			νR1 + νR2 + νR3 + νR5 + ρR4
30	672.17(15.72)	669.04(10.66)	663(80.74)	607(28.14)	νR1 + νR2 + νR3 + νR5
31	705.36(1.89)	702.62(8.46)			τR4 + τR5 + ωRO27H
32	706.44(4.05)	716.34(0.38)			νR1 + νR2 + νR3 + νR5
33	714.31(1.16)	720.74(9.36)			νR2 + νR3 + νR4 + νR5
34	735.57(0.82)	775.89(50.30)			τR4 + τR5 + ωO27H + ωC(R2)H + ωC(R3)H
35	742.37(2.84)	785.15(64.58)	738(57.44)		τR4 + ωO27H + ωC(R2)H + ωC(R3)H
36	752.36(81.78)	791.67(55.69)			ωC(R5)H + ωO27H
37	762.78(57.66)	795.54(6.30)			ωC(R2)H + ωC(R3)H + ωC(R5)H
38	795.46(55.33)	824.74(3.31)	795(74.54)		ωO27H + ωC(R5)H + τR4
39	807.60(16.03)	845.23(8.03)	812(73.86)		ωC(R2)H + τR1
40	826.09(22.02)	849.44(30.23)	835(85.74)		ωC(R1)H
41	828.75(0.99)	862.84(36.42)			νR1 + νR2 + νR3 + νR4 + νR5
42	847.60(0.35)	890.60(10.49)			τR1 + τR2 + τR3 + τR1 + τR4
43	851.12(1.46)	932.85(123.67)			τR5
44	852.95(8.19)	958.18(0.05)			νR5
45	925.59(1.26)	973.66(3.09)			τR5
46	943.26(0.02)	974.48(0.32)			τR2
47	964.82(0.08)	976.20(1.73)			τR3
48	977.30(1.77)	981.05(3.14)			νR4 + νR5
49	979.38(0.24)	1022.64(0.33)			τR5
50	986.69(2.04)	1024.26(0.36)			νR2 + νR3 + νR4
51	989.26(0.21)	1030.44(0.12)			τR2
52	1002.12(0.36)	1030.94(5.91)			τR3
53	1047.01(5.22)	1042.11(1.38)			νR2 + νR3 + νR4 + ρN4H
54	1050.08(5.92)	1048.51(4.50)			νR2 + νR3
55	1058.61(6.34)	1052.89(9.56)			νR5
56	1086.94(13.00)	1081.37(12.09)	1036(76.44)	996(84.02)	δC(R2)H + δC(R3)H + ρN4H
57	1088.06(11.22)	1092.58(2.59)	1070(71.16)		δC(R2)H + δC(R3)H + δC(R5)H + νR4 + νR5
58	1096.86(4.51)	1097.49(3.35)			νR4 + δC(R2)H + δC(R3)H
59	1139.40(10.88)	1137.69(11.07)	1160(80.02)	1167(150.63)	νR1 + νR4 + δC(R2)H + δC(R3)H + δC(R5)H + ρN4H
60	1150.01(6.53)	1149.73(4.34)			νR1 + νR4 + νR5 + δC(R2)H + δC(R3)H + δC(R5)H
61	1156.34(0.84)	1159.44(4.57)			δC(R2)H + δC(R3)H + δC(R5)H + ρN4H + ρO27H
62	1184.70(12.38)	1205.00(7.89)	1192(81.31)		δC(R5)H
63	1199.59(1.26)	1212.70(5.41)			νR1 + νR2 + νR3 + νR4 + δC(R2)H + δC(R3)H
64	1213.67(26.58)	1221.76(15.84)			νR1 + νR2 + νR3 + νR4 + δC(R2)H + δC(R3)H + δC(R5)H
65	1248.33(4.66)	1264.99(0.71)			νR1 + νR5 + νR2 + νR3 + δC(R2)H + δC(R5)H + ρO27H + ρN4H
66	1265.47(6.41)	1278.95(2.83)			νR1 + δC(R2)H + δC(R3)H + ρC(R5)H + ρO27H
67	1288.04(22.63)	1290.08(91.89)	1259(62.48)	1282(171.55), 1312(170.82)	νR5 + νC21O27 + ρN4H + δC(R5)H
68	1303.59(76.60)	1315.25(13.69)	1296(77.71)		νR1 + νR2 + νR3 + νR4 + νR5 + νC8C15 + νC21O27 + ρN4H + ρO27H + ρC(R2)H + ρC(R3)H + ρC(R5)H
69	1319.36(3.32)	1329.41(6.82)			νR1 + νR2 + νR3 + ρN4H + δC(R2)H + δC(R3)H
70	1327.34(18.40)	1340.05(0.34)			νR1 + νC2N9 + νC21O27 + ρN4H + ρC(R2)H + ρC(R3)H + ρC(R5)H
71	1346.17(45.29)	1359.31(80.17)	1332(79.35)		νR4 + νR5 + νC21O27 + ρN4H + ρC(R2)H + ρC(R3)H
72	1363.20(34.11)	1364.42(6.37)	1356(69.90)	1374(88.38)	νR1 + νR4 + δC(R2)H + δC(R3)H + ρO27H
73	1368.44(13.59)	1374.23(13.02)			νR1 + νR2 + νR3 + νR4 + ρC19H + ρC24H

Table 3 (*continued*)

No.	B3LYP/6-311G**	B3LYP/LANL2DZ	Exp. (IR)	Exp. (Raman)	Assign.
74	1403.66(0.53)	1394.42(43.16)			νR4 + νR5 + ρO27H + ρN4H
75	1418.67(7.74)	1428.66(21.22)			νR1 + νR4 + δC(R2)H + ρC(R3)H + ρC(R5)H + ρO27H
76	1439.63(11.10)	1449.40(69.80)			νR1 + νR4 + δC(R2)H + δC(R3)H + ρC(R5)H + ρN4H
77	1444.67(77.32)	1453.52(34.24)	1411(45.61)		νR4 + ρC(R5)H + ρO27H
78	1462.81(9.43)	1458.80(14.62)			νR1 + νR2 + νR3 + νR4 + ρC(R2)H + ρC(R3)H + ρO27H
79	1478.94(4.95)	1467.30(1.26)	1485(54.45)	1482(61.45)	νR1 + νR2 + νR3 + νR4 + ρC(R2)H + ρC(R3)H + ρC(R5)H
80	1519.83(84.15)	1508.28(106.82)			νC8N9 + νR5 + δC(R5)H
81	1524.54(38.02)	1526.89(16.94)			νC8C15 + νR4 + νR5 + ρO27H + ρN4H
82	1533.49(42.37)	1539.58(13.23)	1511(65.50)	1505(52.72)	νR1 + νR2 + νR3 + νR4 + ρO27H + ρN4H + δC(R2)H + δC(R3)H
83	1539.33(77.67)	1549.94(108.36)			νR1 + νR2 + νR3 + νR4 + νR5 + νC8C15 + ρO27H
84	1574.62(38.10)	1572.70(31.75)	1566(51.55)	1588(109.37)	νR1 + νR2 + νR3 + νR4 + νR5 + νC8C15 + ρO27H + ρN4H
85	1590.52(21.70)	1586.35(23.36)			νR1 + νR2 + νR3 + νR4 + νR5 + νC8C15 + ρO27H + ρN4H
86	1618.60(8.63)	1617.26(2.01)			νR1 + νR2 + νR3 + νR4 + νR5 + ρO27H + ρN4H
87	1627.38(51.32)	1631.00(54.14)	1627(67.48)		νR2 + νR3 + νR4 + νR5 + ρO27H
88	1642.61(1.91)	1654.78(8.64)			νR1 + νR2 + νR3 + νR4
89	1646.54(7.17)	1659.75(6.43)			νR1 + νR2 + νR3 + νR4 + νR5 + ρO27H + ρN4H
90	1665.85(55.71)	1679.06(96.93)	1666(66.95)		νR5 + ρO27H
91	3138.78(29.17)	2942.86(745.07)			νC(R3)H + νC19H
92	3141.12(27.02)	3176.93(16.14)			νC(R2)H + νC24H
93	3154.01(10.39)	3189.46(11.18)	3067(68.30)		νC(R5)H
94	3159.25(15.15)	3197.13(14.54)			νC(R2)H
95	3172.07(7.82)	3200.09(21.56)			νC(R5)H
96	3181.23(14.12)	3204.45(7.33)			νC(R3)H
97	3191.81(15.65)	3219.96(13.62)			νC(R2)H + νC(R5)H
98	3191.94(23.10)	3227.59(23.57)			νC(R2)H + νC(R5)H
99	3197.91(11.66)	3236.43(33.45)			νC(R3)H
100	3199.05(14.44)	3240.42(19.49)			νC(R5)H
101	3304.98(690.03)	3243.39(19.27)	3227(65.63)		νO27H
102	3673.07(46.74)	3699.06(45.40)	3493(78.89)		νN4H
RMS	48.97	57.77			

Abbreviation/symbols: ν, stretching; δ, bending in-plane; τ, torsion; ω, wagging out-of-plane; ρ, wagging in-plane; R1, ring of C1C2C5C11C6C3; R2, ring of C3C6N14C19C13C7; R3, ring of C5C11N18C24C17C12; R4, ring of C1C2N9C8N4; R5, ring of C15C21C26C31C25C20.

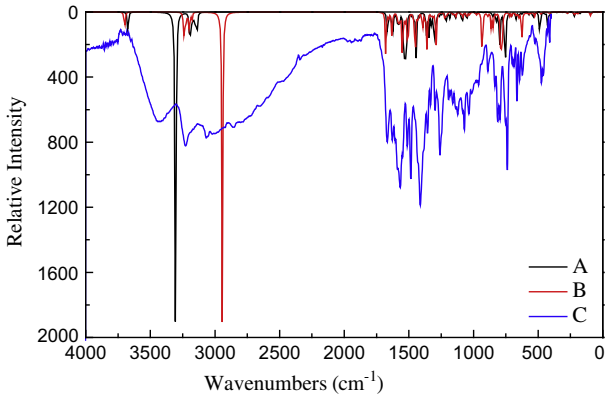

Fig. 3. Calculated IR spectra of title compound by B3LYP/6-311G** (A), B3LYP/LANL2DZ (B), experimental spectrum (C).

and 1505 cm^{-1}, and the computed values are at 1478.94, 1539.33, 1627.38, 1665.85 cm^{-1}. The IR bands at 1296 and 1332 cm^{-1} are mainly due to the C–C stretching vibration of phenyl ring R5, which are strongly coupled with the wagging in-plane motion of N4H and stretching vibration of C21O27. No band corresponding to this vibration is observed in the Raman spectrum, and the computed values are 1303.59 and 1346.17 cm^{-1} with errors of 0.5% and 1.0%. The theoretical values are within experimental error.

The bending vibration of the phenyl ring was observed at 738 cm^{-1} in the IR spectrum and is strongly coupled with out-of-plane C–H wagging of the benzene ring. No band corresponding to this vibration is observed in the Raman spectrum. The theoretical values give 742.37 and 762.78 cm^{-1} and the errors are 0.5% and 3.3%. A medium-strong band at 663 cm^{-1} is assigned to stretching vibrations of all phenyl rings and occurs at 607 cm^{-1} in the Raman spectrum. The data from the B3LYP/6-311G** method show corresponding frequencies of 672.17 and 706.44 cm^{-1}; the errors are 1.4% and 6.5% compared to the experimental value.

In the R4 imidazole ring (ring of C1C2N9C8N4), the ring stretching vibration appears at 1356 cm^{-1} in the IR spectrum. A corresponding, medium-strong Raman band occurs at 1374 cm^{-1}. The theoretical value is 1363.20 cm^{-1} and the error is 0.6%.

C–O, O–H and N–H vibrational modes

The stretching vibration of C21O27 appears at 1259 cm^{-1} in the IR spectrum and at 1282, and 1312 cm^{-1} in the Raman spectrum and the band is strongly coupled with in-plane wagging of N4H and a stretching vibration of phenyl ring R5. The B3LYP/6-311G** method gives a frequency at 1288.04 cm^{-1} and the error is 2.3%. The stretching vibration of O27H appears at 3392 and 3393 cm^{-1} in the literature [35]. In the present work, the stretching vibration of O27H appears at 3227 cm^{-1} in the IR spectrum.

Table 4
the energy levels (eV) of the frontier orbitals of the title compound.

Orbital	Energy			
	B3LYP/6-311G**	B3LYP/LANL2DZ	HF/6-311G**	HF/LANL2DZ
LUMO+6	0.27972	1.04105	4.21401	5.22269
LUMO+5	0.03101	0.09768	3.90763	4.25102
LUMO+4	−0.12843	−0.23890	3.62682	3.56560
LUMO+3	−0.36189	−0.48134	3.18520	3.29214
LUMO+2	−1.30771	−1.45638	2.63855	2.28374
LUMO+1	−1.72321	−1.84892	2.07993	1.74988
LUMO	−1.76865	−1.93381	1.96157	1.58798
HOMO	−5.83627	−5.96389	−7.53907	−7.88192
HOMO−1	−6.55135	−6.57366	−8.62829	−8.92243
HOMO−2	−6.80060	−6.59135	−8.86964	−9.09059
HOMO−3	−6.80522	−6.94209	−9.83342	−10.00185
HOMO−4	−7.24249	−7.03868	−10.48646	−10.64564
HOMO−5	−7.50561	−7.54697	−10.97488	−10.86849
HOMO−6	−7.95049	−8.01824	−11.01760	−11.32752

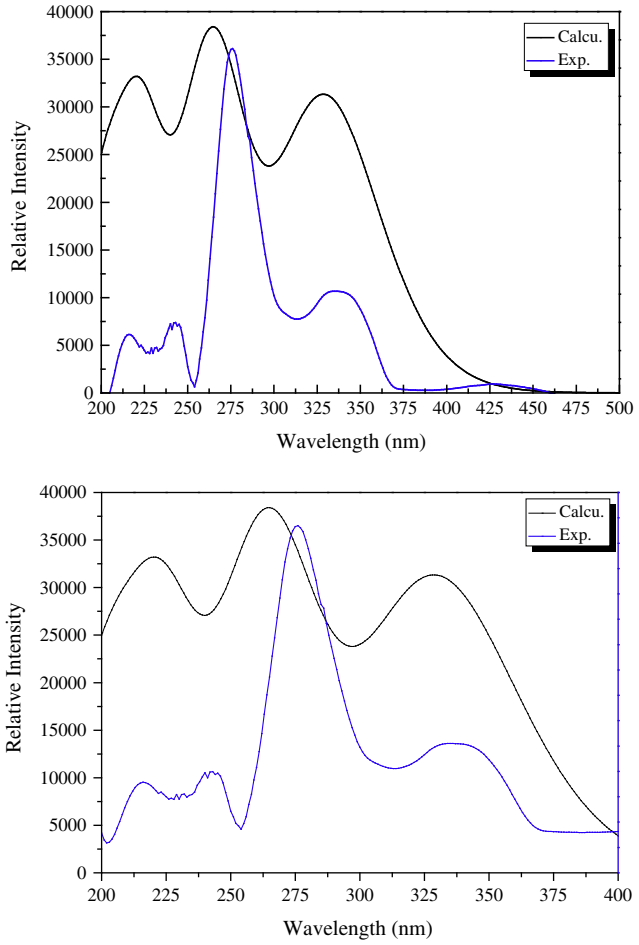

Fig. 4. Experimental and simulated spectra for the title compound in CH_3OH solvent calculated by B3LYP/6-311G**.

No band corresponding to this vibration exists in the Raman spectrum. The B3LYP/6-311G** method gives a value of 3304.98 cm^{-1} and the error is 2.4%. A medium-strong band at 795 cm^{-1} is mainly due to the O27H out-of-plane wagging vibration. No band corresponding to this vibration exists in the Raman spectrum. The B3LYP/6-311G** (795.46 cm^{-1}) method yields an experimental value which is in better agreement than other methods of calculation. The stretching vibration of N4H appears at 3493 cm^{-1} in the IR spectrum. No band corresponding to this vibration exists in the Raman spectrum. The B3LYP/6-311G** (3673.07 cm^{-1}) method overestimates the frequency with an error of 5.2%. The IR band at 1566 cm^{-1} and the corresponding Raman bands at 1588 are assigned to N4H in-plane wagging vibrations and the band is coupled with in-plane C–H bending of the benzene ring. The B3LYP/6-311G** method calculates the frequency to be 1574.62 cm^{-1} and the error is 0.5%. The N4H out-of-plane wagging vibration appears at 475 cm^{-1} in the IR spectrum and the band is coupled with benzene ring torsion vibration. No band corresponding to this vibration exists in the Raman spectrum. The B3LYP/6-311G** method gives a value of 490.13 cm^{-1} and the error is 3.2%.

Electronic spectra

According to the frontier molecular orbital theory, the HOMO, and LUMO orbitals and related orbitals are most important to the electronic properties of compounds. HOMOs usually act as the donors and LUMOs as the acceptors. The energy levels of the frontier orbitals of the compound are listed in Table 4. The experimental and simulated spectra are shown in Fig. 4. The electronic transition energy of the first excited state and the maximum absorption wavelength λ_{max} were obtained by the DFT method. According to the B3LYP/6-311G** method, the energy of the highest occupied molecular orbital (E_{HOMO}) is −5.84 eV, and the energy of the lowest unoccupied molecular orbital (E_{LUMO}) is −1.77 eV. As a result, the $\Delta E_{LUMO-HOMO}$ gap in the compound is about 4.07 eV. On the basis of the optimized geometry in the solvent, calculations show a high-energy band with a peak at 221.3 nm, and a low-energy band with two peaks at 271.7 and 336.6 nm, matching very well with the corresponding experimental absorptions of 237.0, 274.0 and 335.0 nm, respectively. The excited-state which lies at 4.56 eV (271.7 nm), is mainly formed by the H−2 → L + 1, H−1 → L, H → L + 3 transitions. The excited-state which lies at 5.60 eV (221.3 nm), is mainly formed by H−6 → L, H−5 → L + 1, H−2 → L + 3; and the excited-state located at 3.68 eV (336.6 nm) is given by the H → L, H → L + 1 transitions.

Though the simulated spectrum of the title compound in solution has reasonable agreement with the band maximum positions

Table 5
Computed excitation energies (EE), oscillator strengths (f), and electronic transition configurations for the compound.

Exp.	TD-B3LYP/6-311G**			PCM-CH_3OH-TD-B3LYP/6-311G**		
	EE (eV)	f	Config.	EE (eV)	f	Config.
335	336.5(3.68)	0.4394	H → L(57%) H → L+1(38%)	336.6(3.68)	0.4654	H → L(15%) H → L+1(67%)
	309.8(4.00)	0.2040	H−3 → L(18%) H → L+2(67%)	315.0(3.94)	0.3168	H−2 → L(17%) H−1 → L+2(68%)
274	273.3(4.54)	0.2124	H−3 → L(41%) H−3 → L+1(43%) H−1 → L(−24%)	271.7(4.56)	0.2704	H−2 → L+1(62%) H−1 → L(−21%) H → L+3(−18%)
	258.0(4.81)	0.2502	H−3 → L+1(25%) H−3 → L+2(33%) H−1 → L+2(40%)	262.3(4.73)	0.3718	H−2 → L(−31%) H−2 → L+2(19%) H−1 → L+1(−19%) H−1 → L+2(52%)
218	214.8(5.77)	0.1378	H−6 → L(23%) H−5 → L+2(48%) H−1 → L+3(−40%)	221.3(5.60)	0.2160	H−6 → L(56%) H−5 → L+1(−19%) H−2 → L+3(−20%)
	201.9(6.14)	0.2027	H−8 → L(42%) H−8 → L+1(−25%) H−3 → L+6(−21%) H−1 → L+4(−32%)	203.0(6.11)	0.3199	H−8 → L(50%) H−2 → L+5(−22%) H−1 → L+4(−36%)

for the experimental results, the calculation in gas phase was also carried out with the expectation of a better match-up between the simulated and the experimental values. For the optimized geometry in the gas phase, the excited states up to an energy of about 6.70 eV was obtained with the application of TDDFT. The simulated spectrum in gas phase also shows three maximum bands centered at 214.8 nm (5.77 eV), 273.3 nm (4.54 eV) and 336.5 nm (3.68 eV), respectively. Contrary to expectation, the simulated spectrum in gas phase did not agree as well to the experimental values. Excitation energies, oscillator strengths and the corresponding transitions for the optical transition with $f > 0.13$ are reported in Table 5.

Conclusions

2-(1*H*-Imidazo [4,5-*f*][1,10]phenanthrolin-2-yl) phenol has been synthesized and characterized by FT-IR, FT-Raman, UV–vis and X-ray diffraction. Vibrational frequencies were calculated using DFT (B3LYP/6-311G**, B3LYP/LANL2DZ) and HF (HF/6-311G**, HF/LANL2DZ) methods. In assessing the performance of all the levels, it is determined that the observed frequencies are reproduced reasonably well by the DFT (B3LYP/6-311G**, B3LYP/LANL2DZ) and HF (HF/6-311G**, HF/LANL2DZ) calculations. The DFT methods give more reasonable results than the HF methods. The experimental spectrum in CH_3OH solution shows three maximum bands at 237.0, 274.0 and 335.0 nm. The predicted electronic absorption spectra were achieved by TDDFT in gas phase and PCM-TDDFT in CH_3OH solution. The calculated band maximums at 221.3, 271.7, and 336.6 nm in CH_3OH, and 214.8, 273.3, and 336.5 in gas phase provide a good description of the positions of the three band maximums in the observed electronic spectrum. The maximum theoretical values and experimental values very closely match.

Acknowledgements

This work was supported by the Jiangsu Key Laboratory for Chemistry of Low-Dimensional Materials Foundation (Grant No. JSKC12110); National Science Foundation of Educational Commission of Jiangsu Province of China (Grant No. 12KJA150004) and Huaian Key Laboratory for Photoelectric Conversion and Energy Storage Materials (Grant No. HAP201205).

References

[1] P. Biswas, S. Dutta, M. Ghosh, Polyhedron 27 (2008) 2105–2112.
[2] S.S. Ali, Chin. Chem. Lett. 22 (2011) 793–796.
[3] B. Sun, J. Chu, Y. Chen, F. Gao, L.N. Ji, H. Chao, J. Mol. Struct. 890 (2008) 203–208.
[4] J. Jayabharathi, V. Thanikachalam, M.V. Perumal, Spectrochim. Acta Part A Mol. Biomol. Spectrosc. 95 (2012) 614–621.
[5] G. Chelucci, R. Thummel, Chem. Rev. 102 (2002) 3129–3170.
[6] G. Süss-Fink, Dalton Trans. 39 (2010) 1673–1688.
[7] Z.Q. Bian, K.Z. Wang, L.P. Jin, Polyhedron 21 (2002) 313–319.
[8] Q.L. Zhang, J.G. Liu, J. Liu, G.Q. Xue, H. Li, J.Z. Liu, H. Zhou, L.H. Qu, L.N. Ji, J. Inorg. Biochem. 85 (2001) 291–296.
[9] L. Wang, L. Ni, J. Yao, Solid State Sci. 14 (2012) 1361–1366.
[10] N.M. Shavaleev, H. Adams, J.A. Weinstein, Inorg. Chem. Acta 360 (2007) 700–704.
[11] X.L. Wang, Y.Q. Chen, G.C. Liu, J.X. Zhang, H.Y. Lin, B.K. Chen, Inorg. Chem. Acta 363 (2010) 773–778.
[12] Z.D. Xu, H. Liu, S.L. Xiao, M. Yang, X.H. Bu, J. Inorg. Biochem. 90 (2002) 79–84.
[13] D.D. Sun, W.Z. Wang, J.W. Mao, W.J. Mei, J. Liu, Bioorg. Med. Chem. Lett. 22 (2012) 102–105.
[14] T.F. Chen, Y.A. Liu, W.J. Zheng, J. Liu, Y.S. Wong, Inorg. Chem. 49 (2010) 6366–6368.
[15] I.M. Khan, A. Ahmad, M. Aatif, J. Photochem. Photobiol., B 105 (2011) 6–13.
[16] C.W. Jiang, H. Chao, R.H. Li, H. Li, L.N. Ji, Polyhedron 20 (2001) 2187–2193.
[17] L.F. Tan, H. Chao, Y.F. Zhou, L.N. Ji, Polyhedron 26 (2007) 3029–3036.
[18] J. Gao, Z.P. Wang, C.L. Yuan, H.S. Jia, K.Z. Wang, Spectrochim. Acta Part A Mol. Biomol. Spectrosc. 79 (2011) 1815–1822.
[19] B. Sun, Y.C. Wang, C. Qian, J. Chu, S.M. Liang, H. Chao, L.N. Ji, J. Mol. Struct. 963 (2010) 153–159.
[20] G. Chelucci, R.P. Thummel, Chem. Rev. 102 (2002) 3129–3170.
[21] Bruker, SMART (ver. 5.625) and SAINT-plus (ver. 6.22), Bruker AXS Inc., Madison, WI, 2000.
[22] Bruker, SADABS (ver. 2.03), Bruker AXS Inc., Madison, WI, 1999.
[23] Bruker, SHELXTL (ver. 6.10), Bruker AXS Inc., Madison, WI, 2000.
[24] HyperChem Pro. Release 6.03, Hypercube Inc., USA, 2000.
[25] A.D. Becke, Phys. Rev. A 38 (1988) 3098–3100.
[26] C. Lee, W. Yang, R.G. Parr, Phys. Rev. B 37 (1988) 785–789.
[27] N.U. Zhanpeisov, H. Fukumura, J. Phys. Chem. C 111 (2007) 16941–16945.
[28] A. Nicklass, M. Dolg, H. Stoll, H. Preuss, J. Chem. Phys. 102 (1995) 8942–8952.
[29] C. Jarmorski, M.E. Casida, D.R. Salahub, J. Chem. Phys. 104 (1996) 5134–5147.
[30] R. Cammi, J. Tomasi, J. Comput. Chem. 16 (1995) 1449–1458.
[31] M. Frisch, G. W. Trucks, H. B. Schlegel, G. E. Scuseria, M. A. Robb, J. R. Cheeseman, J. A. Montgomery Jr., T. Vreven, K. N. Kudin, J. C. Burant, J. M. Millam, S. S. Iyengar, J. Tomasi, V. Barone, B. Mennucci, M. Cossi, G. Scalmani, N. Rega, G. A. Petersson, H. Nakatsuji, M. Hada, M. Ehara, K. Toyota, R. Fukuda, J. Hasegawa, M. Ishida, T. Nakajima, Y. Honda, O. Kitao, H. Nakai, M. Klene, X. Li, J. E. Knox, H. P. Hratchian, J. B. Cross, C. Adamo, J. Jaramillo, R. Gomperts, R. E. Stratmann, O. Yazyev, A.J. Austin, R. Cammi, C. Pomelli, J. W. Ochterski, P. Y. Ayala, K. Morokuma, G. A. Voth, P. Salvador, J. J. Dannenberg, V. G. Zakrzewski, S. Dapprich, A. D. Daniels, M. C. Strain, O. Farkas, D. K. Malick, A. D. Rabuck, K. Raghavachari, J. B. Foresman, J. V. Ortiz, Q. Cui, A. G. Baboul, S. Clifford, J. Cioslowski, B. B. Stefanov, G. Liu, A. Liashenko, P. Piskorz, I. Komaromi, R. L. Martin, D. J. Fox, T. Keith, M. A. Al-Laham, C. Y. Peng, A. Nanayakkara, M. Challacombe, P. M. W. Gill, B. Johnson, W. Chen, M. W. Wong, C. Gonzalez, J. A. Pople, Gaussian 03, Revision C.02, Gaussian Inc., Wallingford, CT, 2004.
[32] W.Z. Zhang, L. Li, Y.H. Xiao, Acta Crystallogr. Sect. E 64 (2008) o1331.
[33] A. Frisch, A.B. Nielsen, A.J. Holder, Gaussview Users' Manual, Gaussian Inc., 2003.
[34] H.W. Lin, W.X. Zhu, Chin. J. Chem. 21 (2003) 1054–1058.
[35] Z.L. Xu, Y. He, S. Ma, X.Y. Wang, Transition Met. Chem. 36 (2011) 585–591.